

Chapter 4

Halo orbits around L_1 , L_2 and L_3 for Sun-Mars system in the elliptical restricted three body problem with radiation pressure

4.1 Introduction

In Ch. 2, halo orbits around L_1 , L_2 and L_3 are computed in CRTBP framework and effects of perturbations of radiation pressure and oblateness on parameters of halo orbits are analyzed. In solar system, planets and other celestial bodies move in elliptical orbits. So, it becomes necessary to study ERTBP for understanding the behaviour of celestial objects. Researchers (Danby (1964), Bhatnagar and Hallan (1978), Rabe (1973), Meire (1981), Markellos et al. (1992), Roberts (2002), Kumar and Narayan (2012), Györgyey (1985), Kumar and Choudhry (1990), Douskos and Markellos (2006), Suraj et al. (2018), and Hussain and Umar (2019)) have computed libration points of ERTBP and studied their linear and non-linear stability. The study shows that the stability of Lagrangian points is affected due to non-zero value of eccentricity of orbit of primaries. Also, the location and the size of the stability region depends on the value of eccentricity of the orbit of the primaries. This gives motivation for finding halo orbits in ERTBP framework.

For the CRTBP, a significant amount of analytical and numerical work for halo orbits has been performed, whilst relatively fewer analytical results are available for the ERTBP. Luo et al. (2018) have obtained natural formation flying on quasi-halo orbits in photogravitational CRTBP using a method based on ergodic Poincaré mapping. Peng et al. (2017b) have used the Monte Carlo method in a pulsating synodic system for the

study of the maintenance of libration point orbit in elliptic Sun-Mercury model. The Hamiltonian of ERTBP explicitly depends on the independent variable, time, which makes the computation as well as the study of properties of two and three dimensional periodic and quasi-periodic orbits difficult. Palacián et al. (2006) and Neishtadt et al. (2021) have averaged the Hamiltonian of ERTBP with respect to independent variable time for simplifying the computations and obtained new family of periodic orbits in spatial ERTBP. Peng and Xu (2015) and Peng et al. (2017a) have used the numerical technique for finding multi-revolution elliptic halo orbits and studied the stability of these orbits for M5N2, M7N3 and M9N4 resonant orbits.

In ERTBP, independent variable appears explicitly in the equations of motion of infinitesimal body which makes the computation of halo orbits difficult. Lindstedt-Poincaré method is the most commonly used method for finding halo orbits. The solutions obtained using Lindstedt-Poincaré method are revised by applying differential correction method. For simplifying the computations, the eccentric anomaly is considered as independent variable and the equations of motion are averaged with respect to it.

In this chapter, a first guess for halo orbits around collinear Lagrangian points is obtained using the Lindstedt-Poincaré method upto the third order approximation. This analytical solution is taken as an initial guess in differential correction method and a revised, more precise solution is obtained. Further, the more massive primary is considered as a source of radiation and the effects of this perturbation on parameters of halo orbits are analyzed. So, in this study $q_1 = q$ and $q_2 = 1$ is taken in equation (1.25). This model is applied to the Sun-Mars system and bifurcation point of halo orbits from planar Lyapunov orbits for different radiation pressures of the Sun are computed. The stability of halo orbits is studied and the effects of solar radiation on stability region are observed. For bifurcation and stability analysis, natural parameter continuation is used. The variations in size, location, amplitude and period of halo orbits due to radiation pressure are shown graphically. At last, a graphical comparison between halo orbits in CRTBP and ERTBP framework is done which shows the effect of eccentricity of primaries' orbit on parameters of halo orbits. All lengthy expressions appearing in computation of analytic solution are given in Appendix B.

4.2 Computation of halo orbits

The procedure of computation of halo orbits is similar in CRTBP and ERTBP. In ERTBP also, the origin is translated to the Lagrangian point and the new coordinate system is normalized by dividing with the distance γ between the Lagrangian point and the nearest primary as described in Chapter 2. The transformation (2.1) is used to get the coordinates in new coordinate system $\tilde{x}\tilde{y}\tilde{z}$. In this case, γ is the root of the polynomial (1.38), (1.39) or (1.40). Then the equations of motion (1.24) get transformed to

$$\begin{aligned}\tilde{x}'' - 2\tilde{y}' &= \frac{1}{\gamma^2} \frac{\partial \Omega}{\partial \tilde{x}}, \\ \tilde{y}'' + 2\tilde{x}' &= \frac{1}{\gamma^2} \frac{\partial \Omega}{\partial \tilde{y}}, \\ \tilde{z}'' &= \frac{1}{\gamma^2} \frac{\partial \Omega}{\partial \tilde{z}},\end{aligned}\tag{4.1}$$

where

$$\Omega = \frac{1}{\sqrt{1-e^2}} \left[\frac{1}{2} \left((\gamma\tilde{x} - \mu + 1 \mp \gamma)^2 + (\gamma\tilde{y})^2 \right) + \frac{(1-\mu)q}{R_1} + \frac{\mu}{R_2} \right],\tag{4.2}$$

$$R_1 = \sqrt{(\gamma\tilde{x} + 1 \mp \gamma)^2 + (\gamma\tilde{y})^2 + (\gamma\tilde{z})^2},\tag{4.3}$$

$$R_2 = \sqrt{(\gamma\tilde{x} \mp \gamma)^2 + (\gamma\tilde{y})^2 + (\gamma\tilde{z})^2},\tag{4.4}$$

for L_1 and L_2 . And for L_3 ,

$$\Omega = \frac{1}{\sqrt{1-e^2}} \left[\frac{1}{2} \left((\gamma\tilde{x} - \mu - \gamma)^2 + (\gamma\tilde{y})^2 \right) + \frac{(1-\mu)q}{R_1} + \frac{\mu}{R_2} \right],\tag{4.5}$$

$$R_1 = \sqrt{(\gamma\tilde{x} - \gamma)^2 + (\gamma\tilde{y})^2 + (\gamma\tilde{z})^2},\tag{4.6}$$

$$R_2 = \sqrt{(\gamma\tilde{x} - \gamma - 1)^2 + (\gamma\tilde{y})^2 + (\gamma\tilde{z})^2}.\tag{4.7}$$

In (4.2), the upper sign corresponds to L_1 and the lower sign corresponds to L_2 . By using the generating function relation (2.11) of the classical Legendre polynomials for expansion of $1/R_1$ and $1/R_2$, system (4.1) gets transformed to (Koon et al. (2011, p.146)):

$$\begin{aligned}
 \tilde{x}'' - 2\tilde{y}' - (\alpha + 2b_2)\tilde{x} &= \frac{\partial}{\partial \tilde{x}} \sum_{m \geq 3} b_m \nu^m P_m \left(\frac{\tilde{x}}{\nu} \right), \\
 \tilde{y}'' + 2\tilde{x}' + (b_2 - \alpha)\tilde{y} &= \frac{\partial}{\partial \tilde{y}} \sum_{m \geq 3} b_m \nu^m P_m \left(\frac{\tilde{x}}{\nu} \right), \\
 \tilde{z}'' + b_2\tilde{z} &= \frac{\partial}{\partial \tilde{z}} \sum_{m \geq 3} b_m \nu^m P_m \left(\frac{\tilde{x}}{\nu} \right),
 \end{aligned} \tag{4.8}$$

where

$$\begin{aligned}
 \alpha &= \frac{1}{\sqrt{1-e^2}}, \\
 \nu^2 &= \tilde{x}^2 + \tilde{y}^2 + \tilde{z}^2, \\
 b_m &= \frac{1}{\gamma^3 \sqrt{1-e^2}} \left[(1-\mu)q(-1)^m \left(\frac{\gamma}{1 \mp \gamma} \right)^{m+1} + (\pm 1)^m \mu \right], \quad m \geq 0, \quad \text{for } L_1 \text{ and } L_2,
 \end{aligned}$$

and for L_3 ,

$$b_m = \frac{1}{\gamma^3 \sqrt{1-e^2}} \left[(1-\mu)q + \mu \left(\frac{\gamma}{1+\gamma} \right)^{m+1} \right], \quad m \geq 0.$$

In the expansion of $1/R_1$ and $1/R_2$, the terms containing the products of Legendre polynomials are neglected. In system (4.8), the left hand side has all linear terms and non-linear terms in \tilde{x} , \tilde{y} and \tilde{z} are collected on the right hand side. The solution of the linear system corresponding to the non-linear system (4.8) is given by

$$\begin{aligned}
 \tilde{x}(E) &= A_1 e^{\chi E} + A_2 e^{-\chi E} + A_3 \cos \lambda E + A_4 \sin \lambda E, \\
 \tilde{y}(E) &= -\kappa_1 A_1 e^{\chi E} + \kappa_1 A_2 e^{-\chi E} - \kappa_2 A_3 \sin \lambda E + \kappa_2 A_4 \cos \lambda E, \\
 \tilde{z}(E) &= c_1 \cos \sqrt{b_2} E + c_2 \sin \sqrt{b_2} E,
 \end{aligned} \tag{4.9}$$

where A_1, A_2, A_3, A_4, c_1 and c_2 are arbitrary constants. The quantities χ, λ, κ_1 and κ_2 are given by

$$\begin{aligned}
 \chi &= \sqrt{\frac{-(4-b_2-2\alpha) + \sqrt{16+9b_2^2-16\alpha-8b_2}}{2}}, \\
 \lambda &= \sqrt{\frac{(4-b_2-2\alpha) + \sqrt{16+9b_2^2-16\alpha-8b_2}}{2}}, \\
 \kappa_1 &= \frac{\alpha + 2b_2 - \chi^2}{2\chi}, \\
 \kappa_2 &= \frac{\lambda^2 + \alpha + 2b_2}{2\lambda}.
 \end{aligned}$$

Since χ and $-\chi$ are two real roots of the characteristic equation of the linearized system having same magnitude and opposite signs, the solution (4.9) is unbounded. For getting a bounded solution, the values of A_1 and A_2 are taken to be zero. Also, remaining arbitrary constants are selected as: $A_3 = -A_{\tilde{x}} \cos \phi$, $A_4 = A_{\tilde{x}} \sin \phi$, $c_1 = A_{\tilde{z}} \sin \psi$, $c_2 = A_{\tilde{z}} \cos \psi$. Then solution (4.9) can be expressed as:

$$\begin{aligned}\tilde{x}(E) &= -A_{\tilde{x}} \cos(\lambda E + \phi), \\ \tilde{y}(E) &= \kappa A_{\tilde{x}} \sin(\lambda E + \phi), \\ \tilde{z}(E) &= A_{\tilde{z}} \sin(\sqrt{b_2} E + \psi).\end{aligned}\tag{4.10}$$

Here, $\kappa = \kappa_2$; $A_{\tilde{x}}$, λ , ϕ , respectively, are the in-plane amplitude, frequency and phase; $A_{\tilde{z}}$, $\sqrt{b_2}$, ψ are out-of-plane amplitude, frequency and phase, respectively. Since the in-plane and out-of-plane frequencies are not equal, quasi-periodic Lissajous orbits are obtained if the ratio of these frequencies is irrational. For getting periodic orbits, in this case (ERTBP) also the last equation of system (4.8) is expressed in the form

$$\tilde{z}'' + \lambda^2 \tilde{z} = \frac{\partial}{\partial \tilde{z}} \sum_{m \geq 3} b_m \nu^m P_m \left(\frac{\tilde{x}}{\nu} \right) + \Delta \tilde{z},\tag{4.11}$$

where $\Delta = \lambda^2 - b_2$ is the frequency correction term.

4.2.1 Analytic computation of halo orbits using Lindstedt-Poincaré method

As described in Chapter 2, the non-linear terms of system (4.8) give rise to secular terms in successive approximations. So, the new independent variable $\tau = \omega E$, ω being the frequency connection term, is considered. Then system (4.8) in terms of new independent variable τ can be expressed as (Richardson (1980) and Thurman and Worfolk (1996))

$$\begin{aligned}\omega^2 D^2 \tilde{x} - 2\omega D \tilde{y} - (\alpha + 2b_2) \tilde{x} &= \frac{\partial}{\partial \tilde{x}} \sum_{m \geq 3} b_m \nu^m P_m \left(\frac{\tilde{x}}{\nu} \right), \\ \omega^2 D^2 \tilde{y} + 2\omega D \tilde{x} + (b_2 - \alpha) \tilde{y} &= \frac{\partial}{\partial \tilde{y}} \sum_{m \geq 3} b_m \nu^m P_m \left(\frac{\tilde{x}}{\nu} \right), \\ \omega^2 D^2 \tilde{z} + \lambda^2 \tilde{z} &= \frac{\partial}{\partial \tilde{z}} \sum_{m \geq 3} b_m \nu^m P_m \left(\frac{\tilde{x}}{\nu} \right) + \Delta \tilde{z},\end{aligned}\tag{4.12}$$

where D denotes differentiation with respect to τ . System (4.12) is obtained by replacing the last equations of system (4.8) with the equation (4.11). For finding the third order approximate solution, series in system (4.12) is expanded upto $m = 4$. Then we

get,

$$\begin{aligned}\omega^2 D^2 \tilde{x} - 2\omega D \tilde{y} - (\alpha + 2b_2) \tilde{x} &= \frac{3}{2} b_3 (2\tilde{x}^2 - \tilde{y}^2 - \tilde{z}^2) + 2b_4 \tilde{x} (2\tilde{x}^2 - 3\tilde{y}^2 - 3\tilde{z}^2), \\ \omega^2 D^2 \tilde{y} + 2\omega D \tilde{x} + (b_2 - \alpha) \tilde{y} &= -3b_3 \tilde{x} \tilde{y} - \frac{3}{2} b_4 \tilde{y} (4\tilde{x}^2 - \tilde{y}^2 - \tilde{z}^2), \\ \omega^2 D^2 \tilde{z} + \lambda^2 \tilde{z} &= -3b_3 \tilde{x} \tilde{z} - \frac{3}{2} b_4 \tilde{z} (4\tilde{x}^2 - \tilde{y}^2 - \tilde{z}^2) + \Delta \tilde{z}.\end{aligned}\tag{4.13}$$

Consider the solution of the system (4.13) in the perturbation form as (Thurman and Worfolk (1996)) given in equations (1.41)-(1.44). Since we want to find the third order solution, the series in equations (1.41)-(1.44) are terminated after three terms. Then the solution will have following form:

$$X(\tau) = \epsilon X_1(\tau) + \epsilon^2 X_2(\tau) + \epsilon^3 X_3(\tau),\tag{4.14}$$

$$Y(\tau) = \epsilon Y_1(\tau) + \epsilon^2 Y_2(\tau) + \epsilon^3 Y_3(\tau),\tag{4.15}$$

$$Z(\tau) = \epsilon Z_1(\tau) + \epsilon^2 Z_2(\tau) + \epsilon^3 Z_3(\tau),\tag{4.16}$$

and

$$\omega = 1 + \epsilon \omega_1 + \epsilon^2 \omega_2 + \epsilon^3 \omega_3.\tag{4.17}$$

Using (4.14)-(4.17) into third order equations (4.13) and equating the coefficients of ϵ , ϵ^2 and ϵ^3 , the first, second and third order solutions are obtained, respectively.

The first order equations

Equating the coefficients of ϵ , the first order equations are obtained as

$$\begin{aligned}D^2 \tilde{x}_1 - 2D \tilde{y}_1 - (\alpha + 2b_2) \tilde{x}_1 &= 0, \\ D^2 \tilde{y}_1 + 2D \tilde{x}_1 + (b_2 - \alpha) \tilde{y}_1 &= 0, \\ D^2 \tilde{z}_1 + \lambda^2 \tilde{z}_1 &= 0.\end{aligned}\tag{4.18}$$

The periodic solutions of above system are given by

$$\begin{aligned}\tilde{x}_1(\tau) &= -A_{\tilde{x}} \cos(\lambda\tau + \phi), \\ \tilde{y}_1(\tau) &= \kappa A_{\tilde{x}} \sin(\lambda\tau + \phi), \\ \tilde{z}_1(\tau) &= A_{\tilde{z}} \sin(\lambda\tau + \psi).\end{aligned}\tag{4.19}$$

The second order equations

Incorporating the first order solutions (4.19) of the system (4.18) into the equations of motion (4.13) and then equating the coefficients of ϵ^2 , the second order equations are

computed as

$$\begin{aligned} D^2\tilde{x}_2 - 2D\tilde{y}_2 - (\alpha + b_2)\tilde{x}_2 &= \gamma_{21}, \\ D^2\tilde{y}_2 + 2D\tilde{x}_2 + (b_2 - \alpha)\tilde{y}_2 &= \gamma_{22}, \\ D^2\tilde{z}_2 + \lambda^2\tilde{z}_2 &= \gamma_{23}, \end{aligned} \quad (4.20)$$

where

$$\begin{aligned} \tau_1 &= \lambda\tau + \phi, \quad \tau_2 = \lambda\tau + \psi, \\ \gamma_{21} &= 2\omega_1\lambda A_{\tilde{x}}(\kappa - \lambda) \cos \tau_1 + \alpha_1 + \gamma_1 \cos 2\tau_1 + \gamma_2 \cos 2\tau_2, \\ \gamma_{22} &= 2\omega_1\lambda A_{\tilde{x}}(\lambda\kappa - 1) \sin \tau_1 + \beta_1 \sin 2\tau_1, \\ \gamma_{23} &= 2\omega_1\lambda^2 A_{\tilde{x}} \sin \tau_2 + \delta_1 \sin(\tau_1 + \tau_2) + \delta_1 \sin(\tau_2 - \tau_1), \end{aligned}$$

and remaining coefficients are given in Appendix B. Since the solution of the linearized system corresponding to the system (4.13) is already considered while obtaining the second order equations (4.20), it is sufficient to find particular integral of the system (4.20). The secular terms appearing in the particular integral can be removed by setting $\omega_1 = 0$. Then the solutions of the system (4.20) are

$$\begin{aligned} \tilde{x}_2(\tau) &= \rho_{20} + \rho_{21} \cos 2\tau_1 + \rho_{22} \cos 2\tau_2, \\ \tilde{y}_2(\tau) &= \sigma_{21} \sin 2\tau_1 + \sigma_{22} \sin 2\tau_2, \\ \tilde{z}_2(\tau) &= \kappa_{21} \sin(\tau_1 + \tau_2) + \kappa_{22} \sin(\tau_2 - \tau_1). \end{aligned} \quad (4.21)$$

All the coefficients appearing in the solution (4.21) are given in Appendix B.

The third order equations

By embedding the solutions of the first and second order equations into system (4.13) and equating the coefficients of ϵ^3 , the third order equations can be obtained as

$$\begin{aligned} D^2\tilde{x}_3 - 2D\tilde{y}_3 - (\alpha + 2b_2)\tilde{x}_3 &= \gamma_{31}, \\ D^2\tilde{y}_3 + 2D\tilde{x}_3 + (b_2 - \alpha)\tilde{y}_3 &= \gamma_{32}, \\ D^2\tilde{z}_3 + \lambda^2\tilde{z}_3 &= \gamma_{33}, \end{aligned} \quad (4.22)$$

where

$$\begin{aligned} \gamma_{31} &= [\nu_1 + 2\omega_2\lambda A_{\tilde{x}}(\kappa - \lambda)] \cos \tau_1 + \gamma_3 \cos 3\tau_1 + \gamma_4 \cos(2\tau_2 + \tau_1) + \gamma_5 \cos(2\tau_2 - \tau_1), \\ \gamma_{32} &= [\nu_2 + 2\omega_2\lambda A_{\tilde{x}}(\lambda\kappa - 1)] \sin \tau_1 + \beta_2 \sin 3\tau_1 + \beta_3 \sin(2\tau_2 + \tau_1) + \beta_4 \sin(2\tau_2 - \tau_1), \\ \gamma_{33} &= [\nu_3 + (2\omega_2\lambda^2 + \Delta)A_{\tilde{z}}] \sin \tau_2 + \delta_2 \sin 3\tau_2 + \delta_3 \sin(2\tau_1 + \tau_2) + \delta_4 \sin(2\tau_1 - \tau_2), \end{aligned}$$

and remaining coefficients are listed in Appendix B. The terms $\cos \tau_1$, $\sin \tau_1$, $\sin \tau_2$, $\cos(2\tau_2 - \tau_1)$, $\sin(2\tau_2 - \tau_1)$ and $\sin(2\tau_1 - \tau_2)$ appearing in γ_{31} , γ_{32} and γ_{33} generate secular terms in the solution which cannot be removed by just selecting a value of ω_2 . For removing the secular terms from the solution generated due to the last equation of the system (4.22), two conditions must be satisfied. First, the in-plane and out-of-plane phases ϕ and ψ , respectively, are adjusted such that $\sin(2\tau_1 - \tau_2) \approx \sin(\tau_2)$. For this, the relationship between the phases

$$\psi = \phi + \frac{\pi}{2}p, \quad p = 1, 3 \quad (4.23)$$

must be satisfied. Relation (4.23) is called phase angle relation. Using the phase angle relation (4.23) in the expression of γ_{33} , secular terms can be removed from the solution of the last equation of system (4.22) if

$$\nu_3 + (2\omega_2\lambda^2 + \Delta)A_{\bar{z}} - \delta_4 = 0. \quad (4.24)$$

Equation (4.24) is the second condition for removing the secular term from the solution of the last equation of system (4.22) and it is called amplitude constraint relation. The first two equations of system (4.22) are coupled equations, so the secular terms arising in their solution can be removed by using the single condition (Thurman and Worfolk (1996))

$$(\nu_1 + 2\omega_2\lambda A_{\bar{x}}(\kappa - \lambda) - \gamma_5) - \kappa(\nu_2 + 2\omega_2\lambda A_{\bar{x}}(\lambda\kappa - 1) - \beta_4) = 0 \quad (4.25)$$

from which the value of ω_2 can be obtained as

$$\omega_2 = \frac{(\nu_1 - \gamma_5) - \kappa(\nu_2 - \beta_4)}{2\lambda A_{\bar{x}}(\lambda(\kappa^2 + 1) - 2\kappa)}.$$

Simplifying,

$$\omega_2 = s_1 A_{\bar{x}}^2 + s_2 A_{\bar{z}}^2. \quad (4.26)$$

The quantities s_1 and s_2 are given in Appendix B. Substituting above expression of ω_2 in (4.24), the amplitude constraint can be expressed in the form

$$l_1 A_{\bar{x}}^2 + l_2 A_{\bar{z}}^2 + \Delta = 0, \quad (4.27)$$

where l_1 and l_2 are given in Appendix B.

Using conditions (4.23), (4.24) and (4.25) into system (4.22), revised third order equations are

$$\begin{aligned} D^2\tilde{x}_3 - 2D\tilde{y}_3 - (\alpha + 2b_2)\tilde{x}_3 &= \kappa\beta_5 \cos \tau_1 + (\gamma_3 - \gamma_4) \cos 3\tau_1, \\ D^2\tilde{y}_3 + 2D\tilde{x}_3 + (b_2 - \alpha)\tilde{y}_3 &= \beta_5 \sin \tau_1 + (\beta_2 - \beta_3) \sin 3\tau_1, \\ D^2\tilde{z}_3 + \lambda^2\tilde{z}_3 &= (-1)^{\frac{p-1}{2}} (\delta_3 - \delta_2) \cos 3\tau_1, \quad p = 1, 3, \end{aligned} \quad (4.28)$$

where $\beta_5 = \nu_2 + 2\omega_2\lambda A_{\tilde{x}}(\lambda\kappa - 1) - \beta_4$.

The solution of system (4.28) is given by

$$\begin{aligned} \tilde{x}_3(\tau) &= \rho_{31} \cos 3\tau_1, \\ \tilde{y}_3(\tau) &= \sigma_{31} \sin 3\tau_1 + \sigma_{32} \sin \tau_1, \\ \tilde{z}_3(\tau) &= (-1)^{\frac{p-1}{2}} \kappa_{31} \cos 3\tau_1, \quad p = 1, 3. \end{aligned} \quad (4.29)$$

The coefficients ρ_{31} , σ_{31} , σ_{32} and κ_{31} are given in Appendix B.

Final approximation

Final approximate solution for the initial guess of halo orbits can be obtained by substituting the first, second and third order solutions in the equations (4.14)-(4.17). From these expressions, ϵ can be removed by using the transformation $A_{\tilde{x}} \rightarrow A_{\tilde{x}}/\epsilon$ and $A_{\tilde{z}} \rightarrow A_{\tilde{z}}/\epsilon$. Then the final solution becomes (Thurman and Worfolk (1996) and Tiwary and Kushvah (2015))

$$\begin{aligned} \tilde{x}(\tau) &= \rho_{20} - A_{\tilde{x}} \cos \tau_1 + (\rho_{21} - \rho_{22}) \cos 2\tau_1 + \rho_{31} \cos 3\tau_1, \\ \tilde{y}(\tau) &= (\kappa A_{\tilde{x}} + \sigma_{32}) \sin \tau_1 + (\sigma_{21} - \sigma_{22}) \sin 2\tau_1 + \sigma_{31} \sin 3\tau_1, \\ \tilde{z}(\tau) &= (-1)^{\frac{p-1}{2}} (A_{\tilde{z}} \cos \tau_1 + \kappa_{21} \cos 2\tau_1 + \kappa_{22} + \kappa_{31} \cos 3\tau_1), \quad p = 1, 3. \end{aligned} \quad (4.30)$$

Using solution (4.30), the third order approximate solution for halo orbits around collinear Lagrangian points in ERTBP can be obtained.

4.2.2 Numerical computation of halo orbits using Differential Correction method

Analytic solution obtained using equation (4.30) is revised using DC method. For applying DC method, system (1.24) is converted to corresponding first order system of Ordinary Differential Equations (ODEs) and this first order system is solved using the inbuilt function *ode113* of MATLAB with relative tolerance 2.5×10^{-4} and absolute tolerance 10^{-22} . In *ode113*, the analytic solution computed from (4.30) is used as initial condition. Then the numerical solution obtained using *ode113* function

is revised using DC method and this process is repeated till the error between two successive solutions become less than 10^{-12} . In most of the cases, desired accuracy is achieved within five iterations.

System (1.24) can be converted to first ODEs as follows. Let

$$\begin{aligned} x_1 &= x, & x_2 &= y, & x_3 &= z, \\ x_4 &= x', & x_5 &= y', & x_6 &= z'. \end{aligned}$$

Then system (1.24) becomes

$$\begin{aligned} x_1' &= x_4, \\ x_2' &= x_5, \\ x_3' &= x_6, \\ x_4' &= 2x_5 + \frac{1}{\sqrt{1-e^2}} \left[x_1 - \frac{(1-\mu)q(x_1+\mu)}{r_1^3} - \frac{\mu(x_1+\mu-1)}{r_2^3} \right], \\ x_5' &= -2x_4 + \frac{1}{\sqrt{1-e^2}} \left[1 - \frac{(1-\mu)q}{r_1^3} - \frac{\mu}{r_2^3} \right] x_2, \\ x_6' &= -\frac{1}{\sqrt{1-e^2}} \left[1 - \frac{(1-\mu)q}{r_1^3} - \frac{\mu}{r_2^3} \right] x_3. \end{aligned}$$

The Sun-Mars system with eccentricity $e = 0.0935$, the eccentricity of the orbit of the Mars around the Sun, is considered to check the applicability of the model. Here, the Sun is the source of radiation and there is no perturbation due to the Mars. So, $q_1 = q$ and $q_2 = 1$ is substituted in system (1.24) to get above first order system. In Tables 4.1-4.4, a comparison between the state vectors computed using analytic and numerical method at initial time and after half period are given for halo orbits around L_1 . A similar comparison between state vectors of halo orbits around L_2 are given in Tables 4.5-4.8. These state vectors are computed for $q = 1.000, 0.995, 0.990$ and 0.985 . From Tables 4.1-4.8, it can be noted that the y , x' and z' components of state vectors at half period are closer to zero when the analytical solution is revised using the DC method. So, more accurate solution for finding halo orbits can be obtained when the analytical solution is revised using the DC method.

TABLE 4.1: Comparison of states obtained using analytical and differential correction method around L_1 for $q = 1.000$

State using analytical method		State using DC method	
Initial state	State after half period	Corrected initial state	State after half period
x	0.994890816482541	0.994711618935685	0.996043865240266
y	0	0	0.00000000001374
z	0.000535329147915	0.000535329147916	-0.000429082800205
x'	0	0	-0.000000000005635
y'	0.002770811475971	0.004251866925359	-0.004675006070028
z'	0	0	-0.000000000000682

TABLE 4.2: Comparison of states obtained using analytical and differential correction method around L_1 for $q = 0.995$

State using analytical method		State using DC method	
Initial state	State after half period	Corrected initial state	State after half period
x	0.994067728748270	0.993828113947430	0.995637969786564
y	0	0	-0.000000000002392
z	0.000386431273110	0.000386431273110	-0.000304769912957
x'	0	0	0.0000000000009242
y'	0.003162859951976	0.004525074560607	-0.004958253829338
z'	0	0	0.000000000001102

TABLE 4.3: Comparison of states obtained using analytical and differential correction method around L_1 for $q = 0.990$

State using analytical method		State using DC method		
Initial state	State after half period	Corrected initial state	State after half period	
x	0.993000542121834	0.994773889853204	0.992705549625735	0.995134635773246
y	0	-0.000128544752886	0	0.000000000000803
z	0.000238406539104	-0.000204724989545	0.000238406539104	-0.000188355793828
x'	0	-0.000052856171298	0	-0.0000000000003954
y'	0.003659721578572	-0.003883167080180	0.004841414339245	-0.005256224736978
z'	0	0.000021624099834	0	-0.000000000000150

TABLE 4.4: Comparison of states obtained using analytical and differential correction method around L_1 for $q = 0.985$

State using analytical method		State using DC method		
Initial state	State after half period	Corrected initial state	State after half period	
x	0.991654303650766	0.994200883990771	0.991316630363299	0.994568145612804
y	0	-0.000227084988468	0	-0.0000000000005350
z	0.000796330711253	-0.000683465996676	0.000796330711253	-0.000641633125446
x'	0	-0.000099118789619	0	0.0000000000004497
y'	0.004314811373211	-0.004575204425573	0.005316509713293	-0.005723524526005
z'	0	0.000087254025890	0	0.0000000000000596

TABLE 4.5: Comparison of states obtained using analytical and differential correction method around L_2 for $q = 1.000$

State using analytical method		State using DC method	
Initial state	State after half period	Corrected initial state	State after half period
x	1.003830655970692	1.003560647656570	1.005235304940870
y	0	0	0.00000000000555
z	0.001331053342083	0.001331053342083	-0.001778143830844
x'	0	0	-0.000000000002518
y'	0.004664100958227	0.005984840375609	-0.005036061048196
z'	0	0	0.000000000000635

TABLE 4.6: Comparison of states obtained using analytical and differential correction method around L_2 for $q = 0.995$

State using analytical method		State using DC method	
Initial state	State after half period	Corrected initial state	State after half period
x	1.003636195381908	1.003361293591525	1.004554105521303
y	0	0	0.000000000000386
z	0.00113110380065	0.00113110380065	-0.001425823935909
x'	0	0	0.000000000002090
y'	0.003774002987948	0.005441949039049	-0.004672270942730
z'	0	0	0.000000000000554

TABLE 4.7: Comparison of states obtained using analytical and differential correction method around L_2 for $q = 0.990$

State using analytical method		State using DC method	
Initial state	State after half period	Corrected initial state	State after half period
x	1.003346318032331	1.003061888243641	1.003998835142315
y	0	0	0.000000000000001
z	0.001131665165549	0.001131665165549	-0.001422201022170
x'	0	0	0.0000000000002807
y'	0.003457454264410	0.005462080258496	-0.004671326442074
z'	0	0	-0.000000000000500

TABLE 4.8: Comparison of states obtained using analytical and differential correction method around L_2 for $q = 0.985$

State using analytical method		State using DC method	
Initial state	State after half period	Corrected initial state	State after half period
x	1.003113906257322	1.002848377960509	1.003586113736082
y	0	0	-0.000000000000036
z	0.001084539608261	0.001084539608261	-0.001330094959636
x'	0	0	0.0000000000002847
y'	0.003196413599333	0.005369037343016	-0.000171816118792
z'	0	0	-0.000000000000719

4.3 Bifurcation and Stability analysis

Bifurcation of halo orbits from planar Lyapunov orbits can be identified using the eigenvalues of monodromy matrix. Also, these eigenvalues are useful for stability analysis of halo orbits. A State Transition Matrix (STM) evaluated at one orbital period is called monodromy matrix. For a periodic orbit, STM is a 6×6 matrix, so monodromy matrix is a 6×6 matrix. The eigenvalues of this matrix, λ_i , are always in reciprocal pairs and one pair, called the trivial pair, has eigenvalues equal to one (Zimovan (2017) and Vutukuri (2018)). The stability index of a periodic orbit is defined as

$$\nu_i = \frac{1}{2} \left(\lambda_i + \frac{1}{\lambda_i} \right).$$

Since the eigenvalues are in reciprocal pairs, there are three stability indices, ν_1, ν_2 and ν_3 . The stability index corresponding to the trivial pair is $\nu_2 = 1$ and the out of plane stability index is denoted by ν_3 .

4.3.1 Bifurcation analysis

For finding the bifurcation point of halo orbits from planer Lyapunov orbits, a family of planar Lyapunov orbits is obtained. A family of periodic orbits can be generated using natural parameter continuation or pseudo arclength continuation method. Here, natural parameter continuation method is used for generating a family of planar Lyapunov as well as halo orbits. In this method, a solution obtained by revising an analytic guess using a differential correction is considered. Then, one parameter of this revised solution is varied. In most of the cases, variation is made in x_0, y_0, z_0 , time of flight or in a parameter having physical significance. Then, in the existing solution, old value of parameter is replaced by the revised value of parameter and this solution is used as an initial guess in DC method. This will provide a new trajectory in the neighborhood of previously existing trajectory. This process is continued to generate new family members. Here, the parameter which is modified should not be included in the free variable vector (Zimovan (2017)). The algorithm of natural parameter continuation method with increments in x_0 is described below for an arbitrary three dimensional periodic orbit.

1. Using DC method, get a periodic orbit with initial condition

$$\mathbf{x}_{0,j}^* = \begin{bmatrix} x_{0,j} \\ 0 \\ z_{0,j} \\ 0 \\ y'_{0,j} \\ 0 \end{bmatrix}$$

and period T_j . The superscript * refers to a solution modified using DC method. No superscript implies an initial guess.

2. Increase the value of x_0 by a small quantity, say β , which will give a new initial guess of a nearby family member,

$$\mathbf{x}_{0,j+1} = \begin{bmatrix} x_{0,j} + \beta \\ 0 \\ z_{0,j} \\ 0 \\ y'_{0,j} \\ 0 \end{bmatrix}$$

with period T_j . The value of β depends on the sensitivity of the system, but in most of the cases, it is ± 0.0001 dimensionless units.

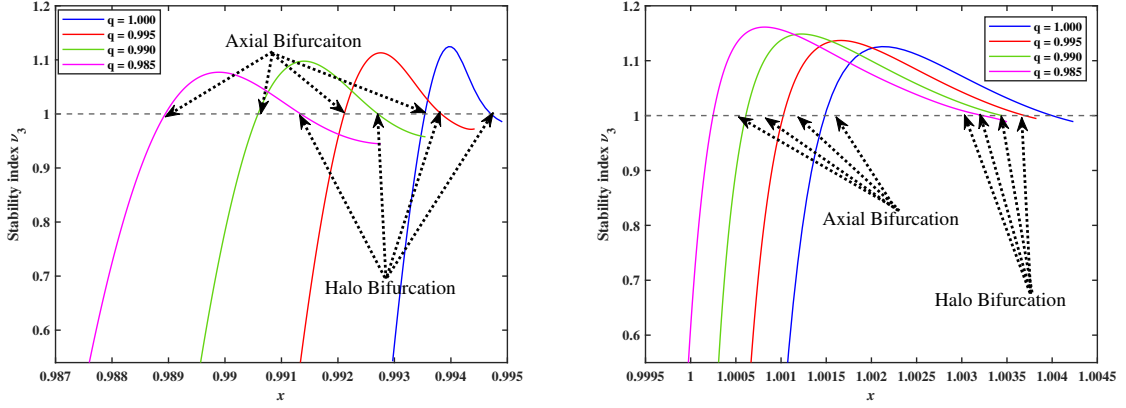
3. Now, use $\mathbf{x}_{0,j+1}$ as an initial guess in DC to obtain a revised nearby solution $\mathbf{x}_{0,j+1}^*$. Here, x -coordinate should not be included in the free variable vector.
4. The DC method gives a nearby solution or a family member, with initial conditions

$$\mathbf{x}_{0,j+1}^* = \begin{bmatrix} x_{0,j} + \beta \\ 0 \\ z_{0,j+1} \\ 0 \\ y'_{0,j+1} \\ 0 \end{bmatrix}$$

with period T_{j+1} .

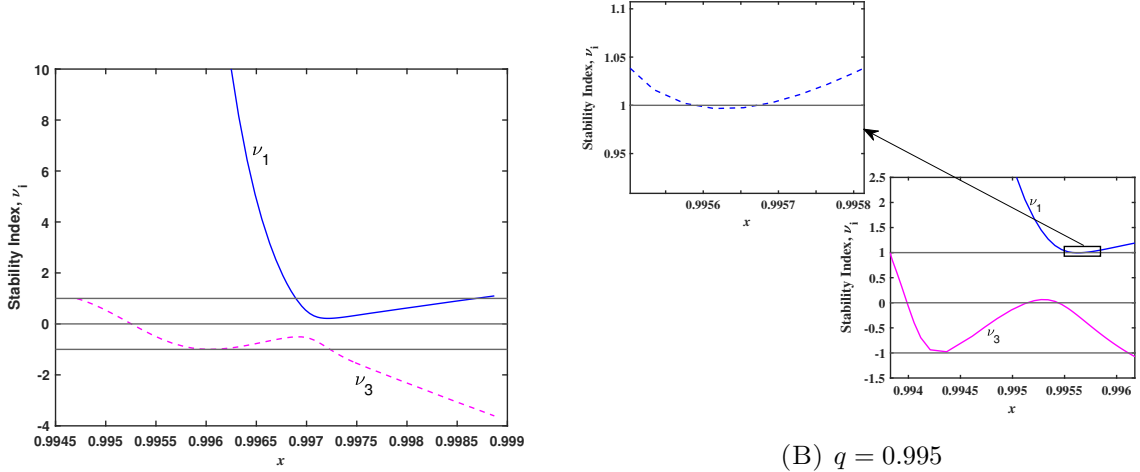
5. This process is repeated to generate the family.

Once the family of planar Lyapunov orbits is generated, the stability indices of each member of this family are obtained. When the stability index of a pair of eigenvalues



(A) L_1 Lyapunov family - out of plane stability index ν_3 (B) L_2 Lyapunov family - out of plane stability index ν_3

FIGURE 4.1: Out of plane stability index ν_3



(A) $q = 1$

(B) $q = 0.995$

FIGURE 4.2: L_1 Halo family stability indices ν_1 and ν_3

crosses the line $\nu = 1$, tangent bifurcation occurs. In this study, two tangent bifurcations occur as out of plane stability index ν_3 crossed the line $\nu_3 = 1$ two times. In Fig. 4.1(A) and Fig. 4.1(B), halo and axial bifurcations around L_1 and L_2 , respectively, are shown for four different values of mass reduction factor (q). Here, the curves of stability index ν_3 corresponding to $q = 1.000, 0.995, 0.990$ and 0.985 are plotted in blue, red, green and magenta colour, respectively. In natural parameter continuation, as we move from the Sun-Mars L_1 towards the Sun, stability index ν_3 increases and crosses the line $\nu_3 = 1$. Here, halo bifurcation occurs. If we further move towards the Sun, the stability index ν_3 attains a maximum and then starts decreasing and again crosses the line $\nu_3 = 1$. Here, axial bifurcation occurs. From Figs. 4.1(A) and 4.1(B), it can be observed that as the radiation pressure increases, the separation between halo and axial bifurcation around L_1 and L_2 increases.

4.3.2 Stability analysis

The linear stability of a periodic orbit can be analyzed from its stability indices. Excluding the trivial pair of eigen values, if remaining two stability indices of an orbit have modulus less than one, then the orbit is stable in linear sense. If either of the stability index has magnitude greater than one, then the orbit is unstable. In Fig. 4.2(A), the stability curves for halo orbits around L_1 with $q = 1$ are plotted. It can be observed from the Fig. 4.2(A) that halo orbits around L_1 are stable when x -coordinate of these orbits lie in the interval $[0.996893099, 0.998688516]$. For $q = 0.995$, the stability curves for halo orbits around L_1 are plotted in Fig. 4.2(B). In this case, the stable orbits lie in the range $0.995590245 \leq x \leq 0.995671331$. From Fig. 4.2, it can be noted that due to radiation of the Sun, the region of stability shrinks and it shifts towards the Sun. Further, a comparison between the present study and classical study done by Howell (1984) shows due to the non-zero value of eccentricity of primaries' orbit, the stability index ν_1 goes closer to zero.

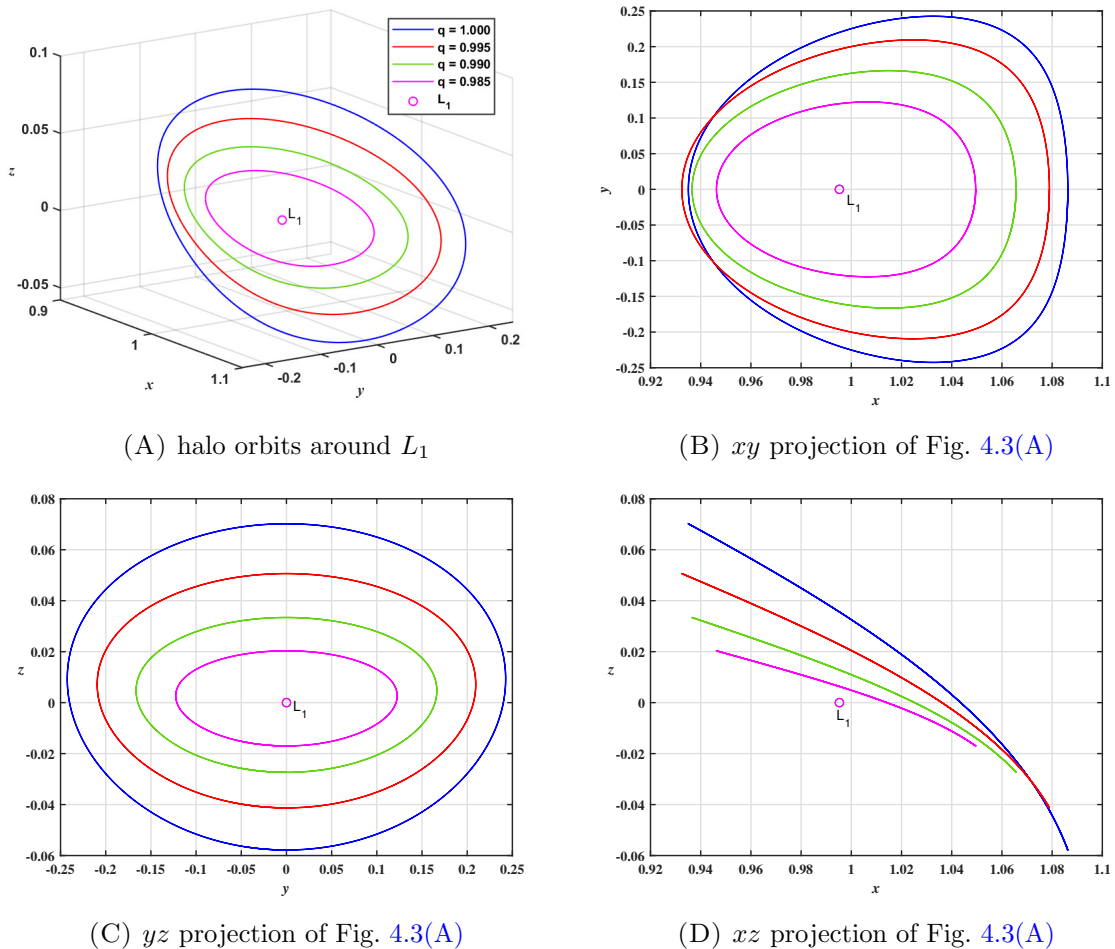


FIGURE 4.3: Variation in size of halo orbits around L_1 against variation in radiation pressure

4.4 Results and Discussion

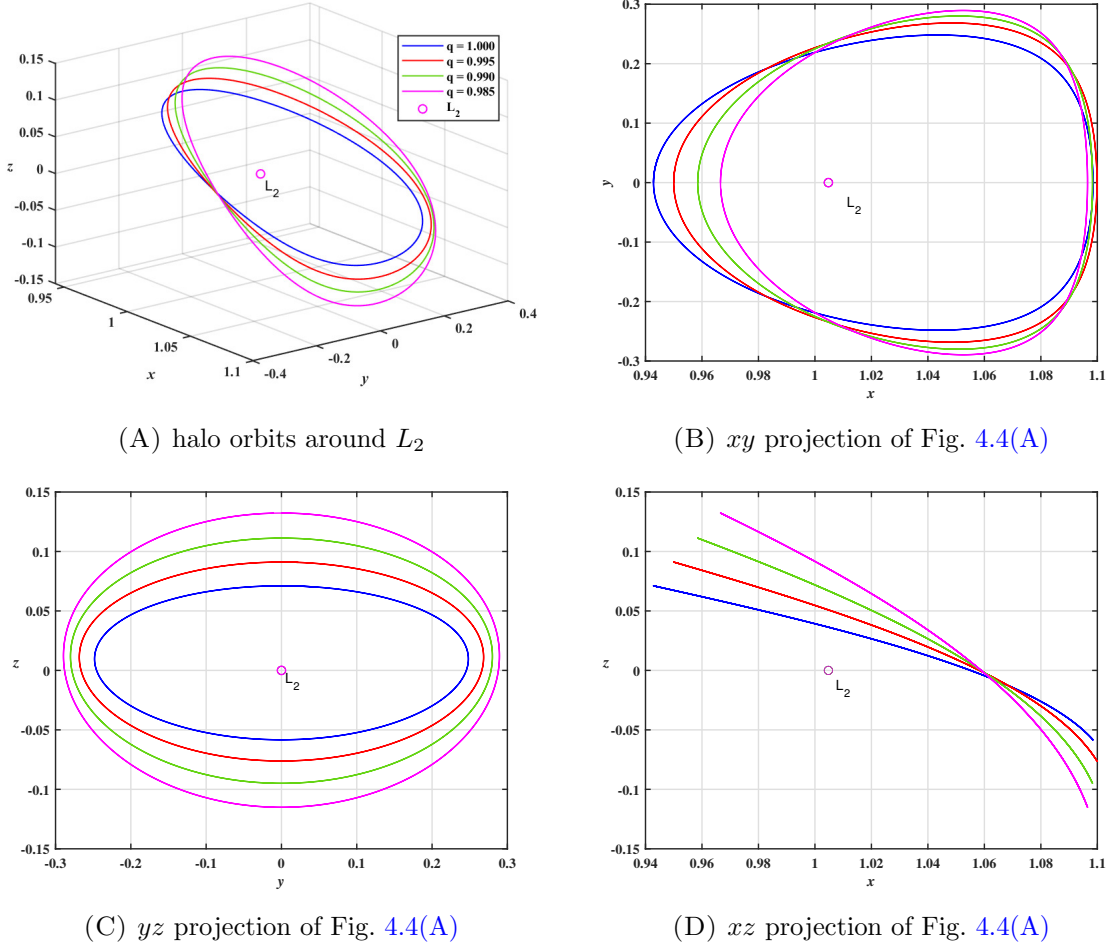
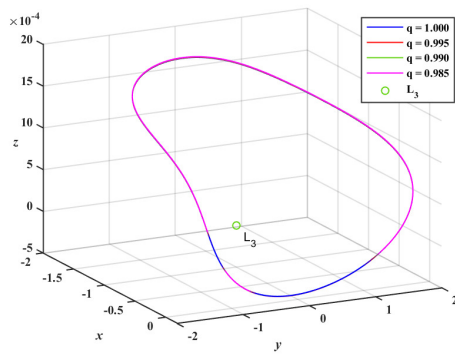
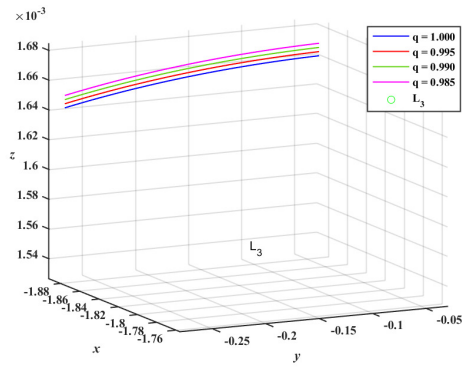


FIGURE 4.4: Variation in size of halo orbits around L_2 against variation in radiation pressure

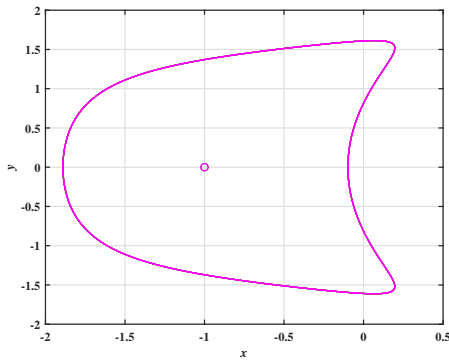
Halo orbits around L_1 , L_2 and L_3 of the Sun-Mars system in ERTBP framework are plotted in a dimensionless synodic coordinate system xyz , having origin at the barycentre of the primaries, for analyzing the effects of solar radiation pressure on parameters of these orbits. By multiplying with the distance between the Sun and the Mars, the orbits in actual dimensions can be obtained. These orbits are plotted using MATLAB by taking $e = 0.0935$, the eccentricity of the orbit of the Mars around the Sun, z -amplitude $A_{\bar{z}} = 1.25 \times 10^6 \text{km}$, phases $\phi = \pi$ and $\psi = \phi + \pi/2$ ($p = 1$). The values of masses of the Sun and the Mars, and the eccentricity of the orbit of the Mars are taken from NASA Fact Sheets for Sun and Mars (<https://nssdc.gsfc.nasa.gov/planetary/factsheet/sunfact.html>, <https://nssdc.gsfc.nasa.gov/planetary/factsheet/marsfact.html>).



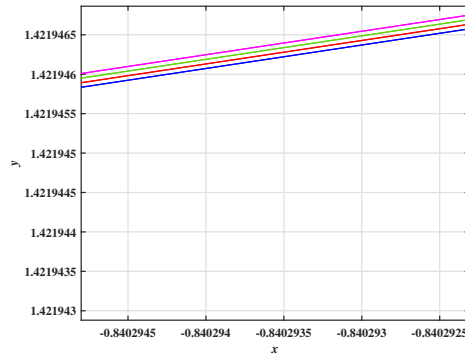
(A) halo orbits around L_3



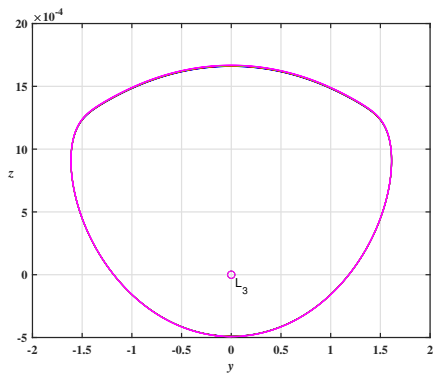
(B) Fig. 4.5(A) zoomed



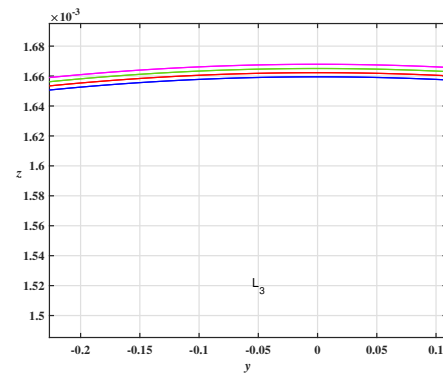
(C) xy projection of Fig. 4.5(A)



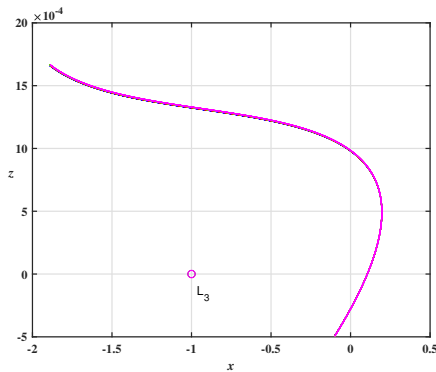
(D) Fig. 4.5(C) zoomed



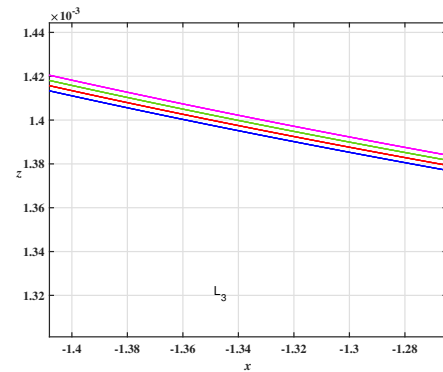
(E) yz projection of Fig. 4.5(A)



(F) Fig. 4.5(E) zoomed



(G) xz projection of Fig. 4.5(A)



(H) Fig. 4.5(G) zoomed

FIGURE 4.5: Variation in size of halo orbits around L_3 against variation in radiation pressure

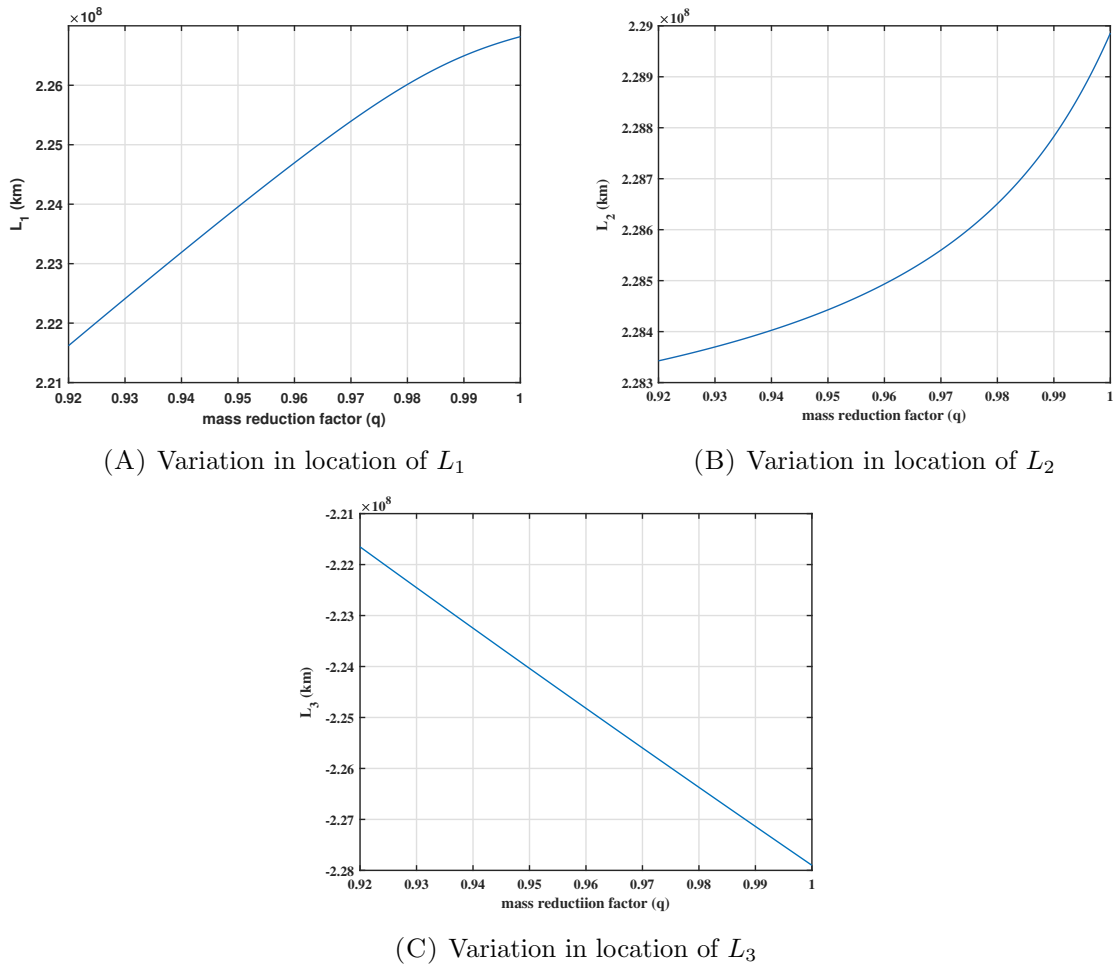
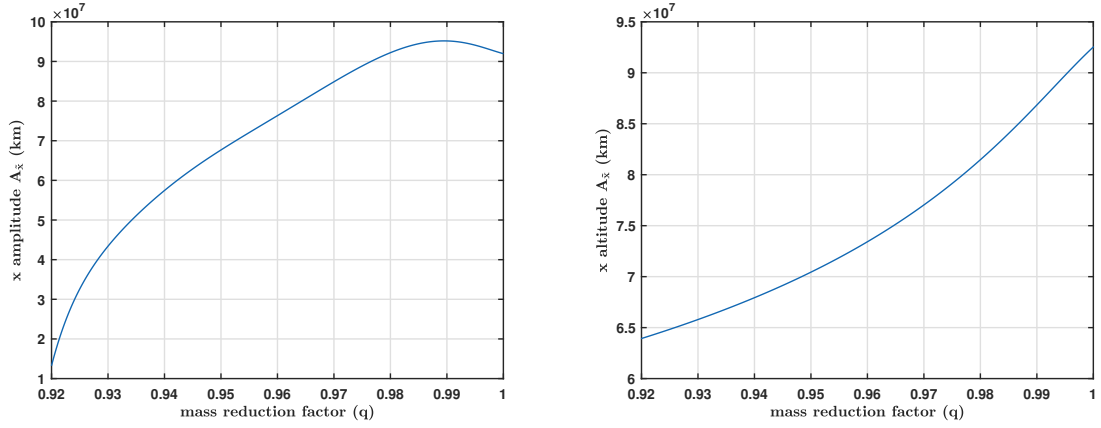


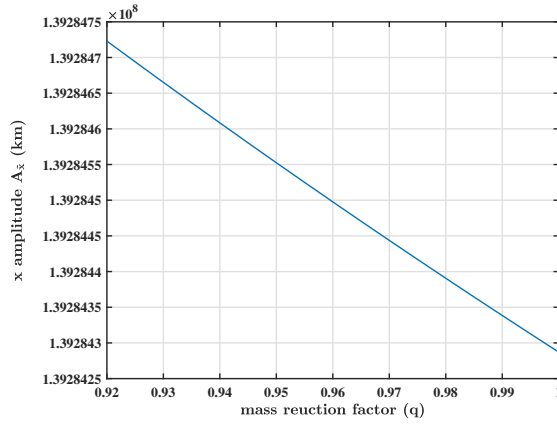
FIGURE 4.6: Variation in location of Lagrangian points against variation in radiation pressure

In Fig. 4.3, Fig. 4.4 and Fig. 4.5, halo orbits around L_1 , L_2 and L_3 , respectively, are plotted for $q = 1.000, 0.995, 0.990$ and 0.985 . In these figures, orbits in blue, red, green and magenta colour correspond to $q = 1.000, 0.995, 0.990$ and 0.985 , respectively. Halo orbits around L_1 are plotted in Fig. 4.3(A) and their xy, yz and xz projections are shown in Figs. 4.3(B), 4.3(C) and 4.3(D), respectively. It can be noted that due to solar radiation pressure, halo orbits around L_1 contract. Fig. 4.4(A) shows halo orbits around L_2 and the two dimensional projections of these orbits are given in Figs. 4.4(B), 4.4(C) and 4.4(D). From Figs. 4.4 and 4.5 it can be concluded that with the increase in the solar radiation pressure, halo orbits around L_2 and L_3 expand.

The change in the location of collinear Lagrangian points due to radiation of the Sun is shown in Fig. 4.6. Here, x -coordinate of Lagrangian point L_i ($i = 1, 2, 3$), in kilometer, is taken on y -axis and the values of mass reduction factor in the interval $[0.92, 1]$ are taken on x -axis. The value $q = 1$ shows that the perturbation due to solar radiation is



(A) Variation in amplitude of orbits around L_1 (B) Variation in amplitude of orbits around L_2

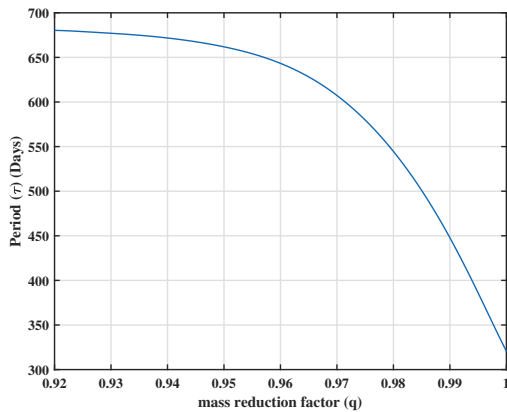


(C) Variation in amplitude of orbits around L_3

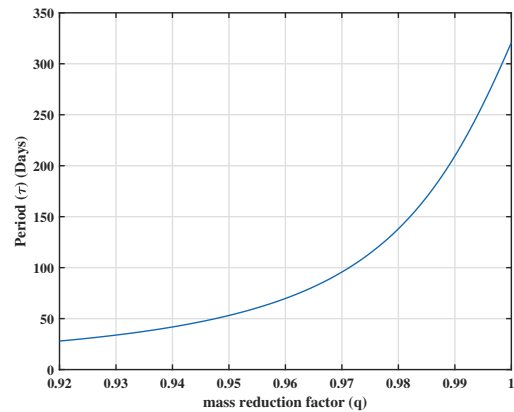
FIGURE 4.7: Variation in amplitude of orbits against variation in radiation pressure

neglected. From Fig. 4.6(A), it can be observed that as the value of q decreases, the x -coordinate of L_1 also decreases which demonstrates that halo orbits around L_1 move closer to the Sun. The x -coordinate of L_2 decreases as the radiation pressure increases, which shows L_2 shifts towards the Mars as well as the Sun. Also, from Fig. 4.6(C), it can be noted that the x -coordinate of L_3 also decreases with the increase in the solar radiation. So, L_3 moves away from the Sun and the Mars due to radiation of the Sun.

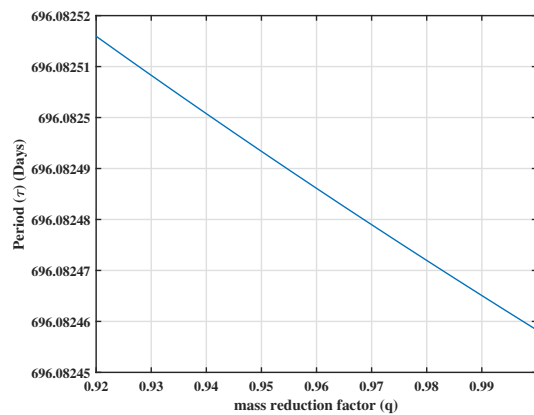
Fig. 4.7 shows the change in the x amplitude of halo orbits around all three collinear Lagrangian points due to change in the radiation pressure. By taking $A_{\bar{z}} = 1.25 \times 10^6$ km, the corresponding value of $A_{\bar{x}}$ is computed using the amplitude constraint relation (4.27). Fig. 4.7(A) shows the value of $A_{\bar{x}}$ increases as the value of q decreases from 1 to 0.9895 but for $0.92 \leq q < 0.9895$, the value of $A_{\bar{x}}$ also decreases with the decrease in q . So, $A_{\bar{x}}$ and q are related by a non-monotonic and non-linear function where as Fig. 4.7(B) shows $A_{\bar{x}}$ is a monotonically decreasing function of q for halo orbits around



(A) Variation in period of orbits around L_1



(B) Variation in period of orbits around L_2



(C) Variation in period of orbits around L_3

FIGURE 4.8: Variation in period of orbits against variation in radiation pressure

L_2 . In this case also, the relationship is non-linear. From Fig. 4.7(C), it is clear that x -amplitude of halo orbits around L_3 increases with the increase in solar radiation pressure.

The effect of radiation on period of halo orbits around collinear Lagrangian points can be analyzed from Fig. 4.8. Due to increase in radiation, period of halo orbits around L_1 and L_3 increases whereas period of halo orbits around L_2 decreases. Fig. 4.8(A) shows that period of halo orbits around L_1 is a non-linear monotonically increasing function of radiation pressure. From Fig. 4.8(B), it can be observed that period of halo orbits around L_2 is a monotonically decreasing function of radiation pressure. In this case also the relation is non-linear. Period of halo orbits around L_3 is a linear monotonically increasing function of solar radiation (Fig. 4.8(C)).

A graphical comparison between halo orbits in CRTBP and ERTBP framework around

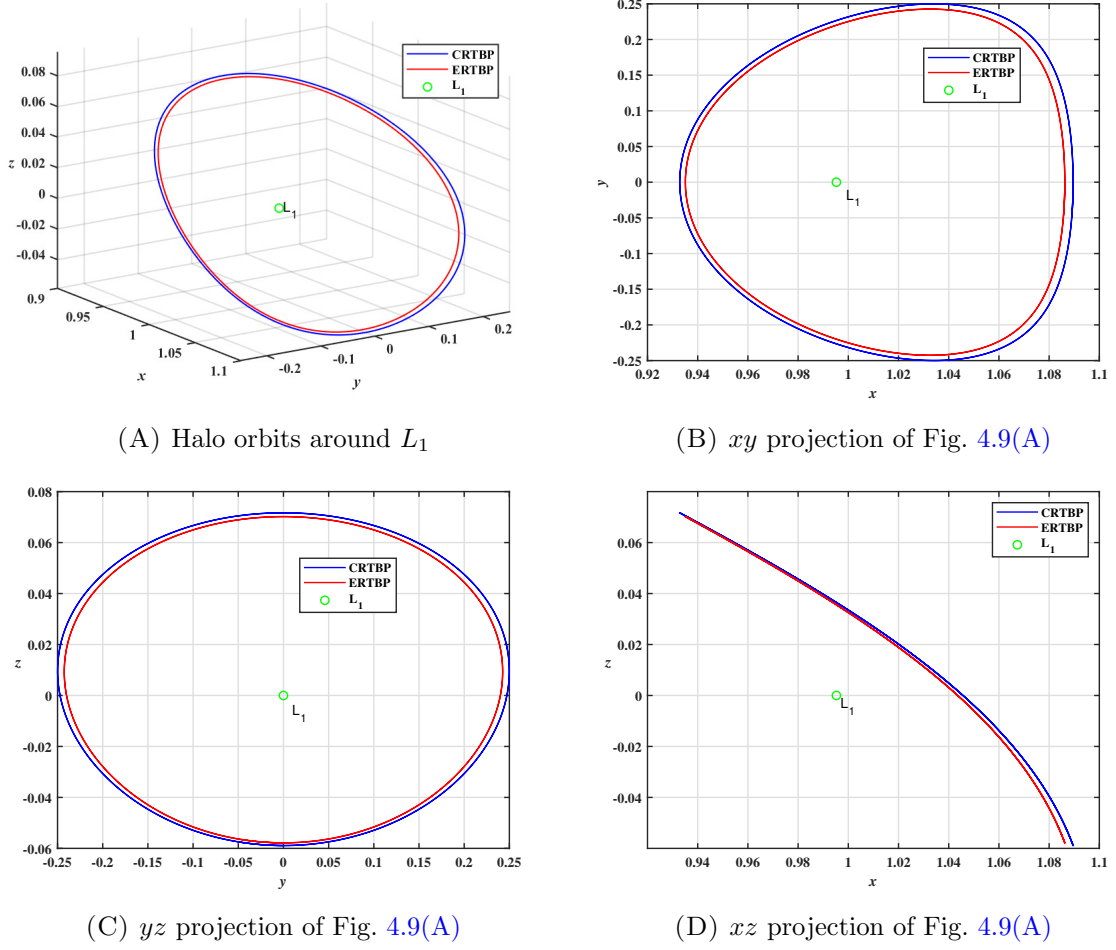
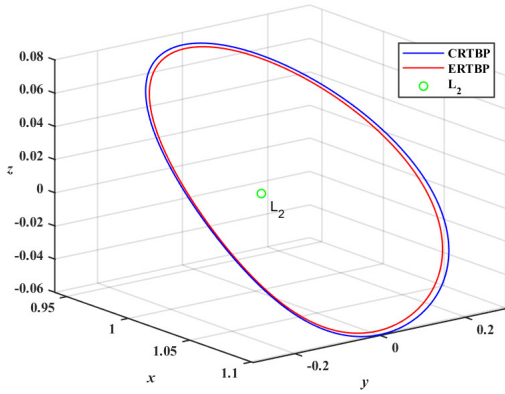


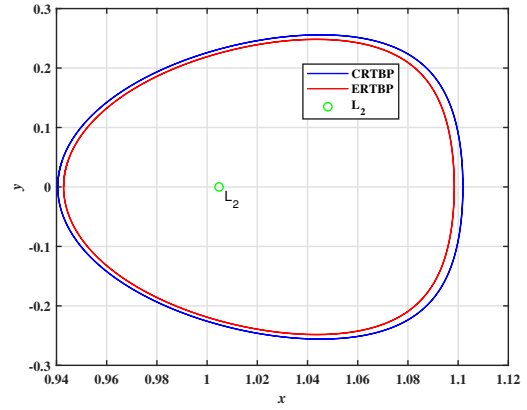
FIGURE 4.9: Variation in size of orbits around L_1 in CRTBP and ERTBP

L_1 is given in Fig. 4.9. The xy , yz and xz projections of halo orbits in Fig. 4.9(A) are given in Figs. 4.9(B), 4.9(C) and 4.9(D), respectively. It is apparent from Fig. 4.9 that halo orbits shrink due to elliptic orbit of the primaries. From Fig. 4.10, similar conclusion can be derived for halo orbits around L_2 also. Here, in Figs. 4.9 and 4.10, orbits in blue represent halo orbits in CRTBP framework and orbits in red represent halo orbits in ERTBP framework.

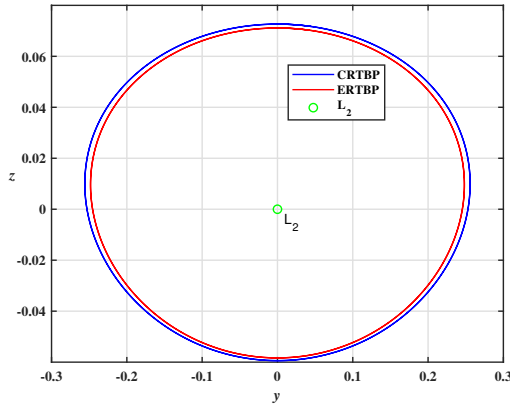
In Fig. 4.11, variation in x -amplitudes of halo orbits around L_1 and L_2 due to perturbation of solar radiation pressure is shown in CRTBP framework. A comparison between values of amplitudes in Fig. 4.7(A) and 4.11(A) shows, amplitude of halo orbits around L_1 in ERTBP framework is smaller than amplitude in CRTBP framework. Similar conclusion for amplitudes of halo orbits around L_2 can be derived from Fig. 4.11(B).



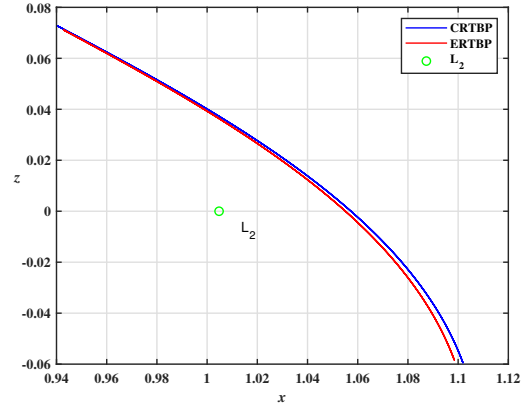
(A) Halo orbits around L_2



(B) xy projection of Fig. 4.10(A)

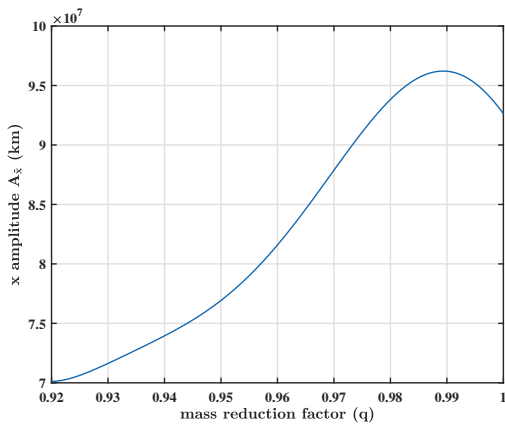


(C) yz projection of Fig. 4.10(A)

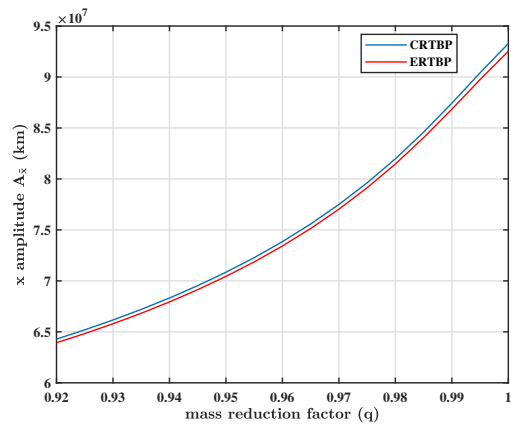


(D) xz projection of Fig. 4.10(A)

FIGURE 4.10: Variation in size of orbits around L_2 in CRTBP and ERTBP



(A) Variation in amplitude of orbits around L_1 against variation in radiation pressure in CRTBP



(B) Variation in amplitude of orbits around L_2 against variation in radiation pressure in CRTBP and ERTBP

FIGURE 4.11: Variation in amplitude of halo orbits around L_1 and L_2

4.5 Conclusions

The Lindstedt-Poincaré method upto the third order approximation is used for getting an initial guess of halo orbits around collinear Lagrangian points L_1 , L_2 and L_3 in the ERTBP framework. This analytic guess is revised using the differential correction method for acquiring more precise initial condition of halo orbits. The constructed model is applied to the Sun-Mars system for finding halo orbits. In this computation, the value of eccentricity $e = 0.0935$, the eccentricity of the orbit of the Mars around the Sun, is considered. Also, the perturbation due to radiation of the Sun is considered to analyze its effects on location of Lagrangian points and parameters of halo orbits.

Using the natural parameter continuation method, the bifurcation for halo and axial orbits from the planar Lyapunov orbits is obtained. Further, the stability analysis of halo orbits is also performed using the same method. The bifurcation analysis shows that due to radiation pressure of the first primary, the separation between the halo and axial bifurcation increases. Also, the radiation of the more massive primary reduces the region of stability of halo orbits.

From the analysis of variations in parameters of halo orbits due to radiation, following conclusions can be made:

- Due to radiation of the more massive primary, halo orbits around L_1 move closer to the first primary, they shrink and their period increase.
- The x -amplitude, $A_{\bar{x}}$, is a non-linear and non-monotonic function of radiation for halo orbits around L_1 .
- Halo orbits around L_2 and L_3 expand with the increase in radiation of the more massive primary.
- As the radiation pressure increases, halo orbits around L_2 shift towards the primaries, their amplitude and period decrease.
- Halo orbits around L_3 move away from the primaries, their amplitude and period increase.

Also, a comparison between halo orbits in ERTBP and CRTBP framework shows that the orbits in ERTBP are smaller than the orbits in CRTBP. Further, the amplitude of orbits in ERTBP is less than the amplitude in CRTBP. The effects of radiation of the more massive primary on parameters of halo orbits are similar in CRTBP and ERTBP. Also, the location of collinear Lagrangian points do not change due to the elliptic orbit of the primaries.